Journal of Colloid and Interface Science 590 (2021) 632–640

Contents lists available at ScienceDirect

Journal of Colloid and Interface Science

journal homepage: www.elsevier.com/locate/jcis

Regular Article

Hierarchical fabrication of hollow Co_2P nanocages coated with $ZnIn_2S_4$ thin layer: Highly efficient noble-metal-free photocatalyst for hydrogen evolution

Quan Zhang, Xiaohao Wang, Juhua Zhang, Lingfeng Li, Huajun Gu, Wei-Lin Dai *

Department of Chemistry and Shanghai Key Laboratory of Molecular Catalysis and Innovative Materials, Fudan University, Shanghai, 200433, PR China

GRAPHICAL ABSTRACT

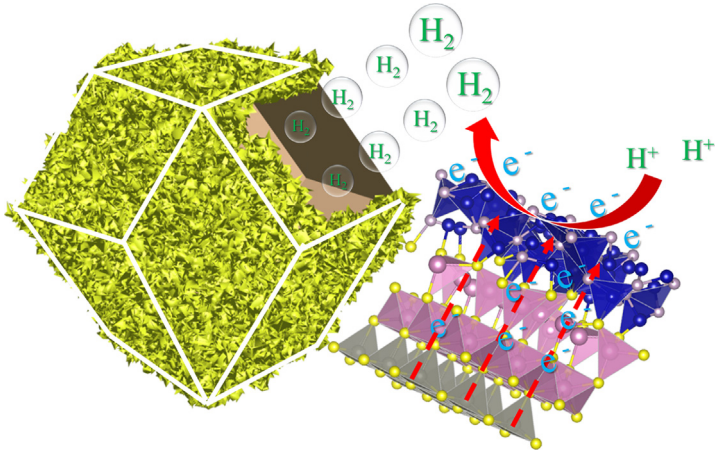

ARTICLE INFO

Article history:
Received 22 December 2020
Revised 18 January 2021
Accepted 25 January 2021
Available online 1 February 2021

Keywords:
ZIF-67
Co_2P NCGs
Co_2P/ZIS NCGs
Interfacial charge transfer
PHE reactions

ABSTRACT

The directional synthesis of transition metal phosphides was considered to be an effective strategy to solve the overdependence of noble metals on photocatalytic hydrogen evolution (PHE) reactions. Inspiringly, this work reported a facile method for constructing hollow Co_2P nanocages (Co_2P NCGs) that derived from ZIF-67 by calcining and phosphiding procedure in nitrogen atmosphere to act as non-noble metal cocatalysts. Followed with further coating thin-layered $ZnIn_2S_4$ (ZIS) on the surface of Co_2P NCGs through a hydrothermal reaction, the hierarchical robust $Co_2P/ZnIn_2S_4$ nanocages (Co_2P/ZIS NCGs) were then delicately fabricated as efficient photocatalysts for PHE reactions. The uniquely hollow structure of Co_2P NCGs largely diffused the photogenerated chargers that induced from ZIS and the closely interfacial contact significantly promoted the separation and transfer of electrons from ZIS to Co_2P according to density functional theory (DFT) calculation, synergistically resulting in an efficient hydrogen generation performance. PHE results showed that an efficient H_2 evolution rate of 7.93 mmol/g/h over 10% Co_2P/ZIS NCGs was achieved, about 10 times higher than that of pristine $ZnIn_2S_4$. More importantly, the hierarchically hollow Co_2P/ZIS NCGs exhibited ascendant PHE activity in comparison with that of 1% noble metal (Pt, Au, Ag) loaded $ZnIn_2S_4$ with superior sustainability, all indicating the efficient and stable photocatalysts of Co_2P/ZIS NCGs for PHE reactions.

* Corresponding author.
E-mail address: wldai@fudan.edu.cn (W.-L. Dai).

https://doi.org/10.1016/j.jcis.2021.01.083
0021-9797/

1. Introduction

The rational use of energy and the permanent protection of environment were still the two major themes of scientific research, which followed then that the development of clean energy, undoubtedly, provided a fundamental pathway for solving these problems [1–6]. Hydrogen, as a kind of clean and high combustion energy, had been paid great attention and high expectations for a long time to realize the lasting prospect of energy utilization [7–9]. Among various hydrogen production strategies, photocatalytic hydrogen evolution (PHE) was proposed to be a viable route to generate sustainably clean hydrogen depending on endless solar energy conversion [10–12]. However, most of the PHE reactions still relied on the cocatalytic role of noble metals, such as Pt, Au and Ag, which greatly limited the economy and feasibility of PHE into real application [13–16]. Hence, the stable and feasible substitution of noble metals with alternative materials was of great significance to boost PHE reactions practically.

Transition metal phosphides (TMPs) were expected to be one of the few materials that could replace noble metals to economically promote the performance of PHE reactions due to its controllable *d*-band center with excellent stability and anti-poisoning property [17,18]. In specifically, cobalt phosphide, as one category of TMPs, had been commonly reported in literatures according to its facile preparation process and wide sources of raw materials [19,20]. Some advanced works had involved cobalt phosphide in enhancing PHE reactions and contributed a lot to the proposal of synthesized methods [21–23], however, most of these instructive works anchored cobalt phosphide as a single active center on the surface of photocatalysts, which greatly restrained the interfacial electron transfer efficiency in reactions. It was acknowledged that the hollow morphology of cocatalyst with large surface exposed benefited a lot for the rapid transfer of electrons in reactions [24–26], and if cobalt phosphide materials with its advantages to substitute noble metals, could be designed to be supported by hollow skeleton and framed in the structure of nanocages, definitely providing an effective mean to achieve the high efficiency of electron transfer for elevating PHE reactions.

As a representative material with suitable band gap and controllable morphology, $ZnIn_2S_4$ (ZIS) based photocatalyst had made great breakthroughs in obtaining high efficiency of PHE reactions [27,28], however, the rapid recombination of chargers and limited light absorption capacity of pristine ZIS were also prominent [29,30]. Therefore, it was a logical and feasible proposal to use the cobalt phosphide nanocages as discussed above to improve the PHE activity of ZIS by comprehensively utilizing the advantages of the two counterparts. Till now, some interesting works had reported the potential application of Co_2P nanoparticle with other materials to achieve efficient PHE reactions [31–33], despite these influential works, the revelation of hollow Co_2P nanocages that encapsulated within self-assembled ZIS thin layer as closely hierarchical heterojunction to replace noble metals and significantly boost PHE reactions, to our best knowledge, were still interesting but had seldom been investigated.

Herein, inspired by above analysis and referred to the preparation tactics developed by Li [34], this work reported a cost-effective method for fabricating ZIF-67 precursors by coordinating Co^{2+} ions with organic ligand 2-methylimidazole and then obtained a hollow Co_2P nanocages (Co_2P NCGs) through calcining and phosphiding in nitrogen atmosphere, which were further conducted as supported frameworks for growing thin-layered ZIS *via* a facially hydrothermal method, finally yielding the hierarchically targeted Co_2P/ZIS NCGs for efficient PHE reactions under simulated sunlight irradiation without noble metal assisted. Additionally, the electron density distributions and possible transfer pathways at the interface of Co_2P and ZIS was deeply analyzed by density functional theory (DFT) calculation.

2. Materials and methods

2.1. Materials

$Co(NO_3)_2{\cdot}6H_2O$ and dimethyl imidazole were purchased from Sigma-Aldrich. Zinc chloride ($ZnCl_2$), indium chloride tetrahydrate ($InCl_3{\cdot}4H_2O$), thioacetamide (TAA) and sodium hypophosphite (NaH_2PO_2) were purchased from Aladdin Bio-Chem Technology Co., Ltd. Methanol, glycerol, sodium sulfide nonahydrate ($Na_2S{\cdot}9H_2O$), sodium sulfite (Na_2SO_3), chloroplatinic acid ($H_2PtCl_6{\cdot}6H_2O$), chloroauric acid ($HAuCl_4{\cdot}4H_2O$), silver nitrate ($AgNO_3$) and sodium sulphate (Na_2SO_4) were purchased from Sinopharm Chemical Reagent Co., Ltd. Deionized (DI) water and ethanol were used as received without further purification.

2.2. Sample preparation

2.2.1. Synthesis of ZIF-67

In a typical procedure, 5.82 g of $Co(NO_3)_2{\cdot}6H_2O$ was dissolved in 200 mL of methanol and stirred vigorously for 30 min to form solution A. Then 6.56 g of dimethyl imidazole was dissolved in another 200 mL of methanol and stirred for 20 min to form solution B, which were quickly transferred to solution A and stirred violently for 10 min to form homogeneous solution. After being aged at room temperature for 24 h, the purple solid products of ZIF-67 were washed three times with methanol and dried overnight under vacuum oven.

2.2.2. Synthesis of Co_3O_4 nanocages

The synthesized ZIF-67 powder was placed in crucible and annealed at 500 °C for 2 h with heating rate of 5 °C min^{-1} under N_2 atmosphere and cooled down to room temperature naturally, resulting in the polyhedral Co_3O_4 nanocages (Co_3O_4 NCGs).

2.2.3. Synthesis of Co_2P nanocages

The above Co_3O_4 precursors were put into the middle of crucible, which was placed behind of another crucible that loaded with 1 g of NaH_2PO_2. The sample was calcined at 300 °C with a ramping rate of 5 °C min^{-1} for 2 h in N_2 atmosphere to obtain the Co_2P nanocages, which were donated as Co_2P NCGs.

2.2.4. Synthesis of $Co_2P/ZnIn_2S_4$ nanocages

Different mass proportions of the above Co_2P NCGs to $ZnIn_2S_4$ (5, 10, 18 and 30%) were designed to prepare the composite $Co_2P/ZnIn_2S_4$ nanocages (Co_2P/ZIS NCGs) via a facilely hydrothermal method. In detail, a certain amount of Co_2P NCGs was dispersed in 8 mL of water and 2 mL of glycerol with ultrasound for 30 min and kept stirring for another 30 min. After totally being dispersed, 0.0816 g of $ZnCl_2$, 0.1758 g of $InCl_3{\cdot}4H_2O$ and 0.09 g of TAA were sequentially added to the above dispersion and stirred vigorously for 30 min. Afterwards, the mixture was placed and heated in an oil bath at 80 °C. After mild agitation for 120 min, the resulting Co_2P/ZIS NCGs were collected by washing with ethanol and drying overnight.

2.2.5. Synthesis of conventional Co_2P nanoparticles

$Co(NO_3)_2{\cdot}6H_2O$ solution (50 mL, 0.05 M) was firstly mixed with NaOH solution (20 mL, 0.25 M) and then continuously stirred for 2 h. The precipitates were washed and dried in vacuum to obtain $Co(OH)_2$ precursor, which was subsequently ground together with NaH_2PO_2 in one mortar. After that, the mixed samples were

annealed at 300 °C for 2 h in nitrogen atmosphere, followed with washing and drying in a vacuum oven to obtain the Co_2P nanoparticles (Co_2P NPs).

2.2.6. Synthesis of $Co_2P/ZnIn_2S_4$ nanoparticles

The synthetic procedure was similar to that of Co_2P/ZIS NCGs, but with the replacement of Co_2P NCGs by Co_2P NPs. The Co_2P/$ZnIn_2S_4$ nanoparticles were donated as Co_2P/ZIS NPs.

2.3. Photocatalytic hydrogen evolution

Photocatalytic hydrogen evolution was triggered in a closed container connecting to a gas and cooling water circulation externally. The light source was a 300 W Xe lamp (Perfect Light, Beijing Co., China) and the temperature was controlled at 20 °C. In detail, 5 mg of the synthesized photocatalyst was added to 100 mL of deionized water containing $Na_2S{\cdot}9H_2O$ (0.35 M) and Na_2SO_3 (0.25 M) as sacrificial agents. After dispersing for 30 min, the composite dispersion was transferred to a quartz reactor and evacuated by a vacuum pump. The hydrogen was sampled by extracting gases every 60 min and monitored using a gas chromatograph fitted with a 5 Å molecular sieve column and a thermal conductivity detector (TCD).

The apparent quantum efficiencies (AQEs) for photocatalytic H_2 evolution was measured using different monochromatic light filter and the AQE was calculated according to the following equation:

$$\mathrm{AQE}\ (\%) = \frac{2 \times \text{number of evolved } H_2 \text{ molecules}}{\text{number of incident photons}} \times 100\%$$

$$= \frac{2 \times n_{H_2} \times N_A \times h \times c}{S \times P \times t \times \lambda} \times 100\%$$

where n_{H2} is the amount of H_2 molecules, N_A is Avogadro constant, h is the Planck constant, c is the speed of light, S is the irradiation area, P is the intensity of irradiation light, which is measured by an optical power meter, t is the photoreaction time, and λ represents the wavelength of monochromatic light.

3. Results and discussion

3.1. Structural characterizations

The schematically synthetic procedure of hierarchical Co_2P/ZIS NCGs was briefly illustrated in Fig. 1. Step 1 showed that the polyhedral structure of Co_3O_4 nanocages (Co_3O_4 NCGs), deriving from calcination of ZIF-67 in nitrogen atmosphere was firstly obtained. After suffering the phosphiding process in furnace, the above Co_3O_4 NCGs were converted to Co_2P NCGs, remaining the polyhedron shape within step 2. Decorating hollow Co_2P NCGs as a support framework to further grow $ZnIn_2S_4$ (ZIS) on its surface *via* a facilely hydrothermal method was the main content in step 3 and it was necessary to point out that this hierarchical Co_2P/ZIS NCGs provided sufficient interface contact to promote charge transfer from ZIS to Co_2P NCGs when PHE reactions occurred.

SEM, TEM and XRD pattern as shown in Fig. S1–S2 proved the successful synthesis of ZIF-67 with polyhedral morphology and fine crystallization. After calcination, the XRD pattern of the resulted products was exhibited in Fig. S3 and the diffraction peak appeared at 36.8° was well consistent with standard Co_3O_4 samples (JCPDS No: 43-1003), indicating oxidized cobalt were the main species after calcining ZIF-67 in nitrogen atmosphere. Moreover, the basically polyhedral structure was retained in the hollow Co_3O_4 nanocages (Co_3O_4 NCGs) (Fig. S4) and mapping profiles further indicated the main oxidized cobalt species (Fig. S5). While suffering phosphiding procedure, the obtained cobalt phosphide products existed in a crystalline state and the characteristic diffraction peak of Co_2P was definitely appeared and surely proved according to XRD pattern (Fig. S6). Additionally, the hollow nanocage structure was consistently maintained (Fig. S7) and the mapping profiles (Fig. S8) evidently confirmed the completed phosphiding process. Generally, the basically polyhedral structure persisted well in the whole synthetic process from ZIF-67 to hollow Co_2P/ZIS NCGs as summarized in Fig. 2 and the comprehensive mapping profiles also indicated the successful coating of ZIS on Co_2P NCGs.

The XRD patterns as shown in Fig. 3(a) demonstrated the hexagonal phase of pristine ZIS (JCPDS No.: 65-2023) [35] and low proportion of Co_2P in Co_2P/ZIS NCGs mainly exhibited the characteristic peak of ZIS. The diffraction peak of Co_2P was constantly invisible even though the additive amount was increased to 30%, which might be caused by the weak crystallinity and encapsulation of ZIS on Co_2P NCGs. The light absorption capacity of Co_2P, ZIS and Co_2P/ZIS NCGs reflecting by UV Vis. DRS spectrum (Fig. 3(b)) indicated a strong visible light absorption of Co_2P in heterojunction with its proportion increased. It was known that ZIS was sensitive to visible light and excited in this band range to produce electrons and hole pairs [36,37], thus the introduction of Co_2P NCGs certainly favored the absorption of incident visible light of ZIS and provided sufficient light source excitation to generate more photoinduced electrons and hole pairs for PHE reactions [38]. Moreover, a slightly decreased bandgap of Co_2P/ZIS composites was observed in comparison with that of pristine ZIS at 2.26 eV (Fig. S9), and this phenomenon also illustrated the interaction between the counterparts and successful formation of Co_2P/ZIS heterostructure. To determine the existing forms of supported carbon skeleton, Raman spectrum of crystalline Co_3O_4 NCGs and Co_2P NCGs were exhibited in Fig. 3(c). The *D* band was associated to lattice defects or disorder states of carbon, while the *G* band represented the E_{2g} vibration mode of sp2 in carbon materials, thus the increased I_D/I_G value in Co_2P NCGs demonstrated the increase of defect sites in phosphiding process [39,40], benefiting the transfer of photogenerated electrons.

The surface composition and chemical state of Co_3O_4, Co_2P and Co_2P/ZIS NCGs were analyzed using X-ray photoelectron spectroscopy (XPS). The XPS survey scans as shown in Fig. S10 proved

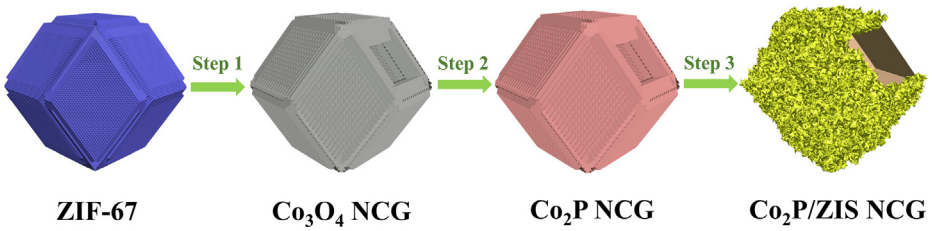

Fig. 1. Schematic illustration of the synthetic process of Co_2P/ZIS NCG.

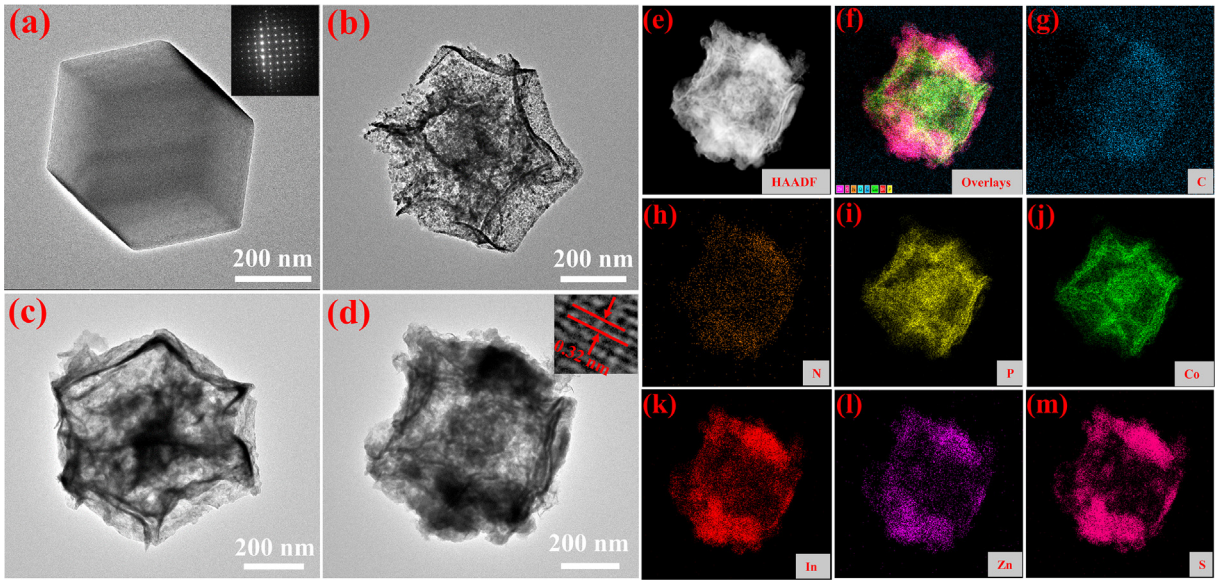

Fig. 2. TEM images of polyhedral ZIF-67 (a), Co_3O_4 NCG (b), Co_2P NCG (c), Co_2P/ZIS NCG (d) and elemental mapping profiles of Co_2P/ZIS NCG (e-m).

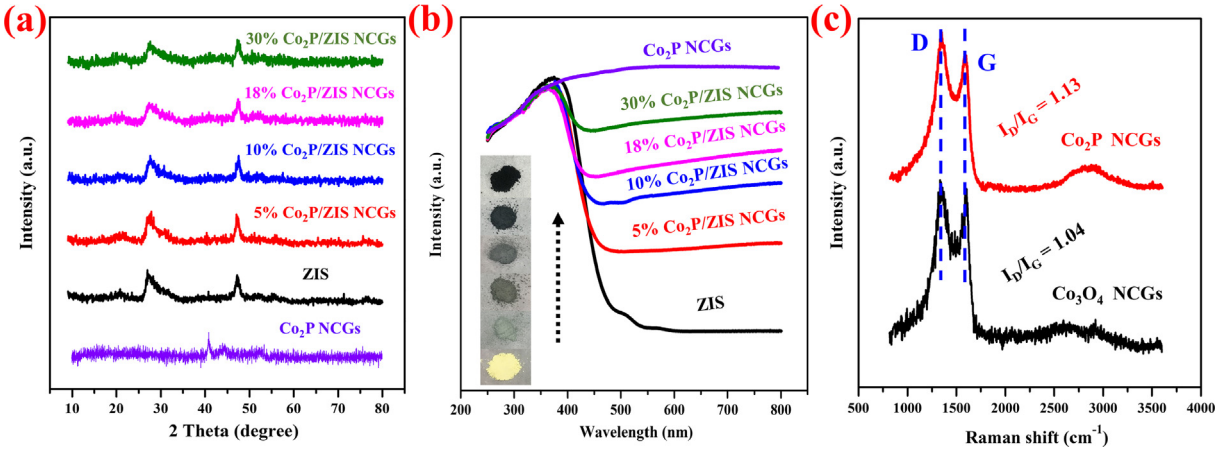

Fig. 3. XRD patterns (a), UV–Vis. DRS spectrum and color display (b) of pristine Co_2P, ZIS and different proportion of Co_2P/ZIS NCGs, Raman spectrum of Co_3O_4 and Co_2P NCGs (c).

the existence of related elements in the synthesized catalysts. In specifically, the high-resolution XPS spectrum of Co 2p, P 2p in different samples and In 3d, S 2p, Zn 2p in Co_2P/ZIS were exhibited in Fig. 4. In Co_3O_4 NCGs (Fig. 4(a)), the binding energy located at 780.3 and 795.6 eV corresponded to the Co 2p 3/2 and Co 2p 1/2, accompanying with the two satellite peaks appeared at 788.0 and 803.1 eV, all proving the main Co-O species [41]. While the higher binding energy of Co 2p 3/2 (781.8 eV), Co 2p 1/2 (797.7 eV) and two satellite peaks (786.2, 803.1 eV) were observed in Co_2P NCGs, indicating there were still partially oxidized state on the surface. However, another two clearly identified peaks, emerging at the binding energy of 778.5 and 793.5 eV, demonstrated the existence of targeted Co-P species [42] and successful phosphiding process for preparing Co_2P NCGs. Though the XPS intensity of Co signal tended to be weaker after coating by ZIS to construct Co_2P/ZIS NCGs, the main Co 2p 3/2 and Co 2p 1/2 species could be clearly distinguished as well, and had slightly shifted to a lower binding energy at 778.1 and 793.1 eV in comparison with that of pristine Co_2P. Generally, the lower binding energy meant a higher electron density [43], thus it could be inferred that the electrons would transfer from ZIS to Co_2P when the Co_2P/ZIS heterojunction formed, illustrating the interfacial interaction between Co_2P and ZIS and acceleration of electron transfer on this occasion. Moreover, the binding energy appeared at 134.6 eV both in Co_2P and Co_2P/ZIS NCGs verified the oxidized states in the surface of catalysts [44], more importantly, the P 2p 3/2 and P 2p 1/2 at the binding energy of 130.4 eV and 131.2 eV sufficiently proved the existence of phosphide state of Co, all further validating the successful phosphiding process as shown in Fig. 4(b). Additionally, the coupled binding energies, fixing at 453.1 and 445.5 eV, 163.5 and 162.5 eV, 1044.7 and 1021.7 eV (Fig. 4(c-e)) could be ascribed to the In 3d 5/2 and In 3d 3/2, S 2p 1/2 and S 2p 3/2, Zn 2p 1/2 and Zn 2p 3/2 in Co_2P/ZIS NCGS [45], respectively. These results fully explained the synthesis and coating of ZIS on Co_2P NCGs. More importantly, comparing with the pristine ZIS, the different binding energy of S 2p and Zn 2p in Co_2P/ZIS NCGS also confirmed the interfacial interaction between Co_2P and ZIS as discussed above. In detail, except for the unchanged binding energy of In 3d, the

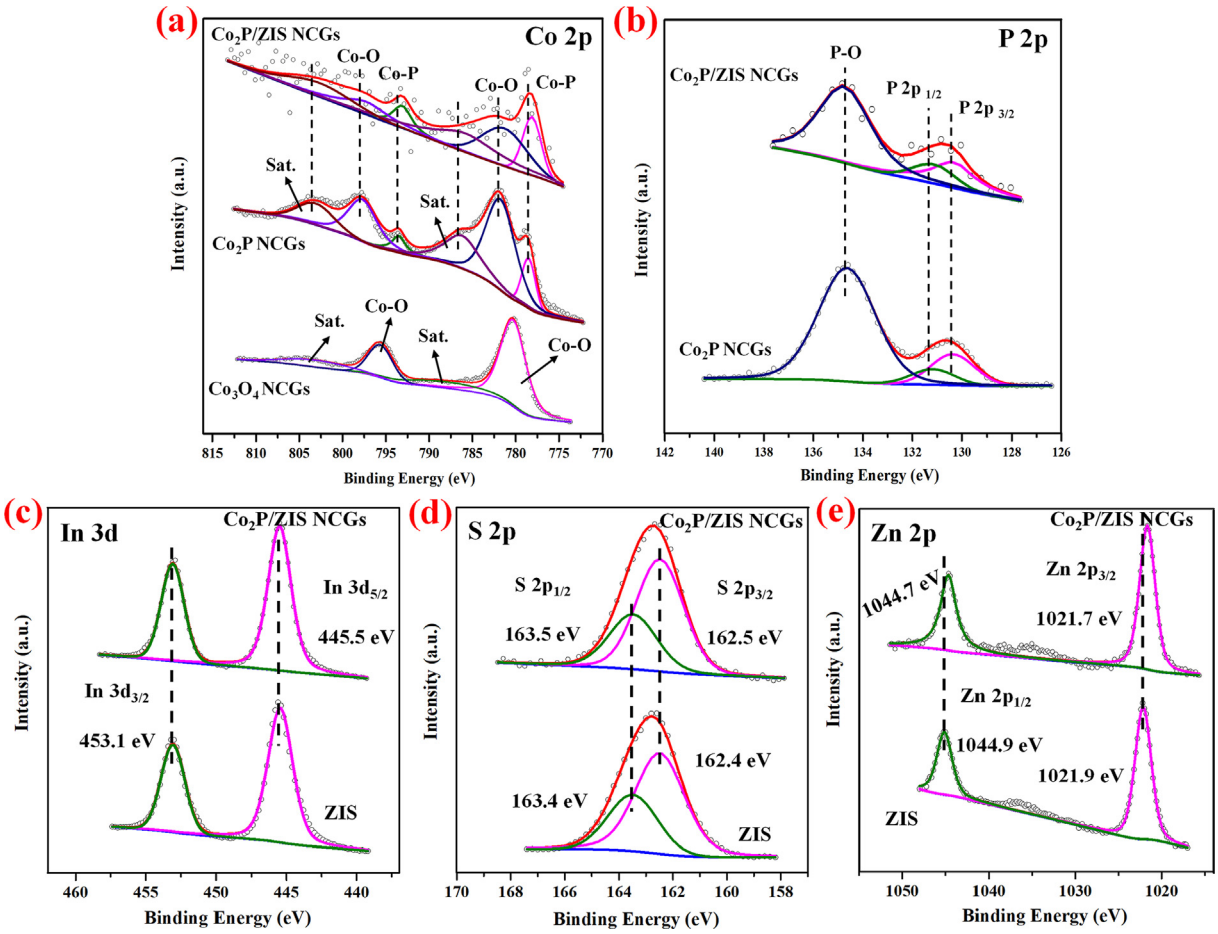

Fig. 4. High-resolution XPS spectrum of Co 2p (a), P 2p (b) in different samples and XPS spectrum of In 3d (c), S 2p (d) and Zn 2p (e) in ZIS and Co_2P/ZIS NCGs.

binding energies of S 2p and Zn 2p in Co_2P/ZIS NCGs were all observed to be changed, where the former slightly increased by 0.1 eV and the latter decreased by 0.2 eV in contrast with that of the pristine ZIS. This phenomenon further proved the mobility of electrons between Co_2P and ZIS [16,36] .

3.2. Photocatalytic hydrogen evolution performance

In general, the Co_2P/ZIS NCGs exhibited superior hydrogen evolution capability than the single counterpart and its PHE performance raised with the increase contents of Co_2P to 10%, but decreased gradually with the excess deposited amounts to 30% as shown in Fig. 5(a-b). The detailed PHE activities of Co_2P, ZIS, 5% Co_2P/ZIS, 10% Co_2P/ZIS, 18% Co_2P/ZIS and 30% Co_2P/ZIS were 0.13, 0.78, 4.72, 7.93, 6.61 and 4.19 mmol/g/h, respectively. In addition, to estimate the PHE level of 10% Co_2P/ZIS NCGs, the performance of noble metal (Pt, Au, Ag) loaded ZIS catalysts and conventional Co_2P nanoparticles encapsulated ZIS (Co_2P/ZIS NPs) for hydrogen generation were investigated and results were shown in Fig. 5(c). It could be seen that the PHE activity of 10% Co_2P/ZIS NCGs was higher than that of 1% noble metals loaded ZIS and 10% Co_2P/ZIS NPs, confirming the feasibility of Co_2P NCGs for solving the overdependence on noble metals in PHE reactions. The detailed performance of noble metals loaded ZIS for enhancing PHE activity could be found in Fig. S11–13 and the successful synthesis of Co_2P/ZIS NPs were proved in Fig. S14–16. The apparent quantum efficiencies (AQEs) over 10% Co_2P/ZIS NCGs for hydrogen generation were measured as shown in Fig. 5(d) and the highest AQEs reached 21.7% at 320 nm monochromatic light. To measure the durability and stability of Co_2P/ZIS catalysts, the recycling stability test and XRD patterns after use were analyzed. The maintained PHE activity in successive five cycles (Fig. 5(e)) and unobvious change of XRD patterns (Fig. 5(f)), where the slight shift of diffraction peak at around 47.2° might be caused by the minor lattice distortion of crystal $ZnIn_2S_4$ under simulated sunlight illumination, pointed out that Co_2P/ZIS NCGs had properties of not only highly sustainable utilization but also good stability and durability.

3.3. Investigation of charge transfer efficiency

To deeply reveal the behavior of charge separation efficiency, the steady-state and time-resolved PL spectrum, the transient photocurrent responses and electrochemical impedance spectra (EIS) of pristine ZIS and Co_2P/ZIS NCGs were correspondingly investigated. The significantly decreased PL quenching plots of Co_2P/ZIS demonstrated the advantageously blocked recombination of photogenerated carriers [47,47] as shown in Fig. 6(a). Moreover, the average lifetime of charge-carrier decay in Co_2P/ZIS NCGs was prolonged to 2.35 ns in comparison with that of pristine ZIS (1.47 ns), further proved the fast transfer of electrons in heterojunctions (Fig. 6(b)). The photocurrent of Co_2P/ZIS heterojunction directly reflected the efficient separation of charges, consequently resulting in a responsive current value comparing with pristine ZIS as exhibited in Fig. 6(c). At the same time, the smaller resistance circles in Co_2P/ZIS samples evidently enabled the fast separation of photoinduced chargers (Fig. 6(d)) than ZIS. All the results summarized

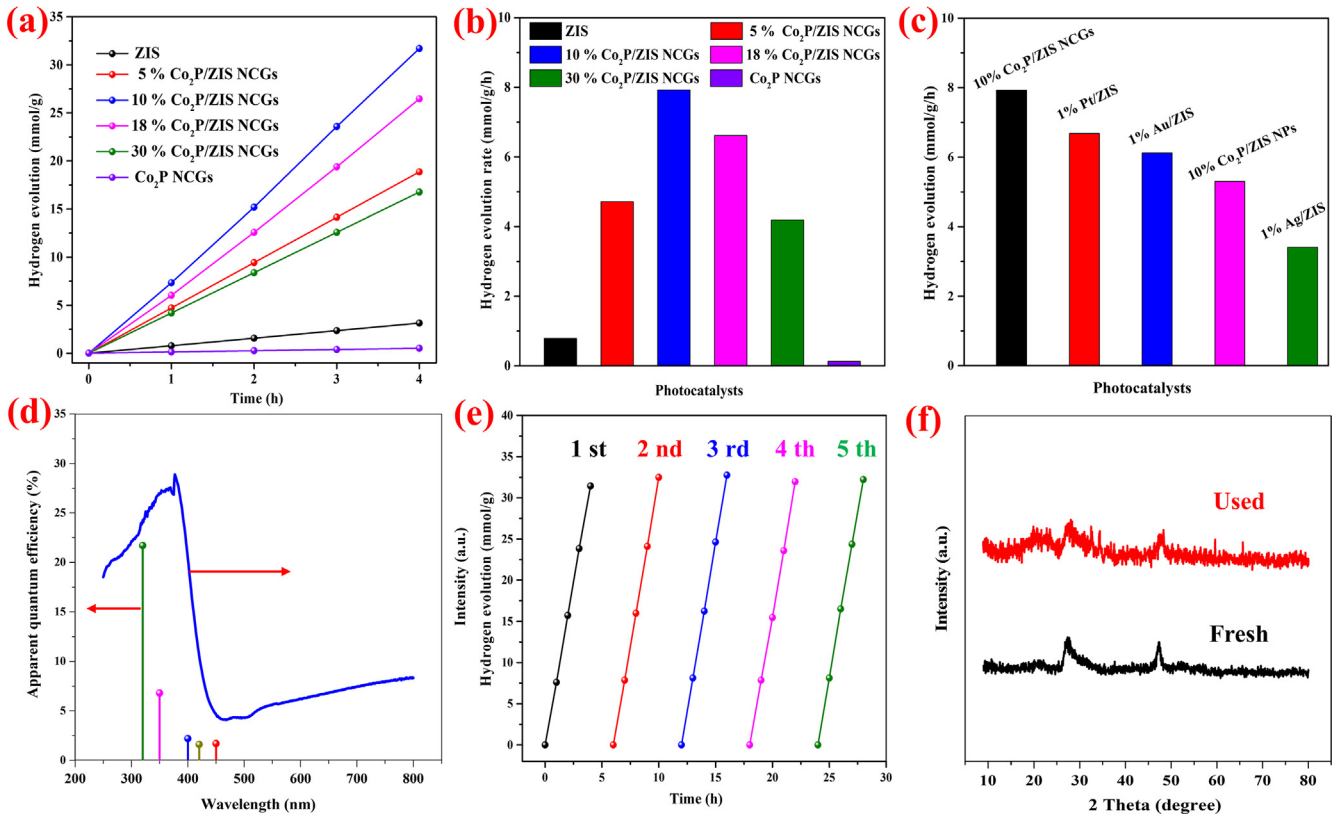

Fig. 5. Time-dependent curves of hydrogen evolution performance (a), hydrogen evolution rate of Co_2P/ZIS NCGs with different proportions (b), comparison of PHE performance with noble metals (Pt, Au, Ag) loaded ZIS and Co_2P/ZIS NPs (c), apparent quantum efficiency over 10% Co_2P/ZIS NCGs (d), recycling stability test (e) and XRD patterns of the fresh and used catalysts (f).

above comprehensively demonstrated the robust charge separation efficiency [48] of Co_2P/ZIS NCGs caused by the formation of interfacial heterojunctions.

3.4. Electron density distribution analysis

To make clear the electronic structures and charge migration pathways, the heterojunction interfaces of $(001)_{Co2P}$ and $(001)_{ZnIn2S4}$ (Fig. S17–S18) were simulated using density functional theory (DFT) calculation. In detail, the four atomically matched structure of Co_2P/ZIS were constructed and the electron density distribution at the interface were theoretically analyzed as shown in Fig. 7. Generally, it could be observed that the accumulated electrons mainly distributed on the surface of Co_2P, while the distribution of deficient electrons were intuitively displayed in ZIS interface, corroborating the strong electron transfer from ZIS to Co_2P at the interfacial heterojunction. And the above calculation results were well consistent with the electron transfer pathways as discussed in XPS part, where the formation of Co_2P/ZIS heterojunction favored the migration of photogenerated electrons from ZIS to Co_2P, thus led to an enhanced PHE performance.

3.5. Photocatalytic mechanism

To determine the conduction band (CB) of each counterpart, Mott-Schottky plots of pristine Co_2P and ZIS sample were correspondingly measured (Fig. 8(a), Fig. S19), and the experimental CB of Co_2P and ZIS was predicted to be −0.48 and −0.51 V, satisfying the electron transfer dynamics. The valence band (VB) of Co_2P (Fig. S20) was estimated at 0.36 V according to $E_{NHE}/V = \Phi + 0.2$ e V −4.44 (E_{NHE}: potential of normal hydrogen electrode and Φ of 4.6 eV: the electron work function of analyzer) [49]. Thus, based on these experimental and theoretical results, the possible working mechanism over hierarchical Co_2P/ZIS NCGs was proposed as shown in Fig. 8(b). The electrons were firstly produced and migrated to the conduction band among the main ZIS photocatalyst under light excitation, while the valence band would be filled with hole pairs. With assistance of the hierarchically designed interfacial contact between ZIS and Co_2P, the electrons generated on CB of ZIS upon sunlight excitation would primarily move to the surface of Co_2P NCGs to reduce protons and release hydrogen, leaving the hole pairs on VB of ZIS to be captured by sacrificial agent. Due to the metalloid attributes and narrow band gap of Co_2P, it then had little contribution to the generation of reductive electrons under light excitation and its positive role was to promote the conduction of electrons on the surface to complete protonation process. Without the timely discharge of electrons by Co_2P NCGs in this photocatalytic system, the recombination of electrons and holes on ZIS would be strongly intensified, leading to an inferior hydrogen generation performance. Moreover, this unique framework of Co_2P NCGs provided more diffused surface area with ZIS and ensured that the chargers could be transferred at the interface, significantly accelerating the electron separation efficiency than that of the single-active noble metal loaded ZIS samples for boosting PHE performance (Fig. 8(c-d)). In general, the fabricated Co_2P nanocages, acting as non-noble metal cocatalysts efficiently accelerated the electron transfer for proton reduction and partially relieved the overdependence of noble metals on photocatalytic hydrogen evolution reactions.

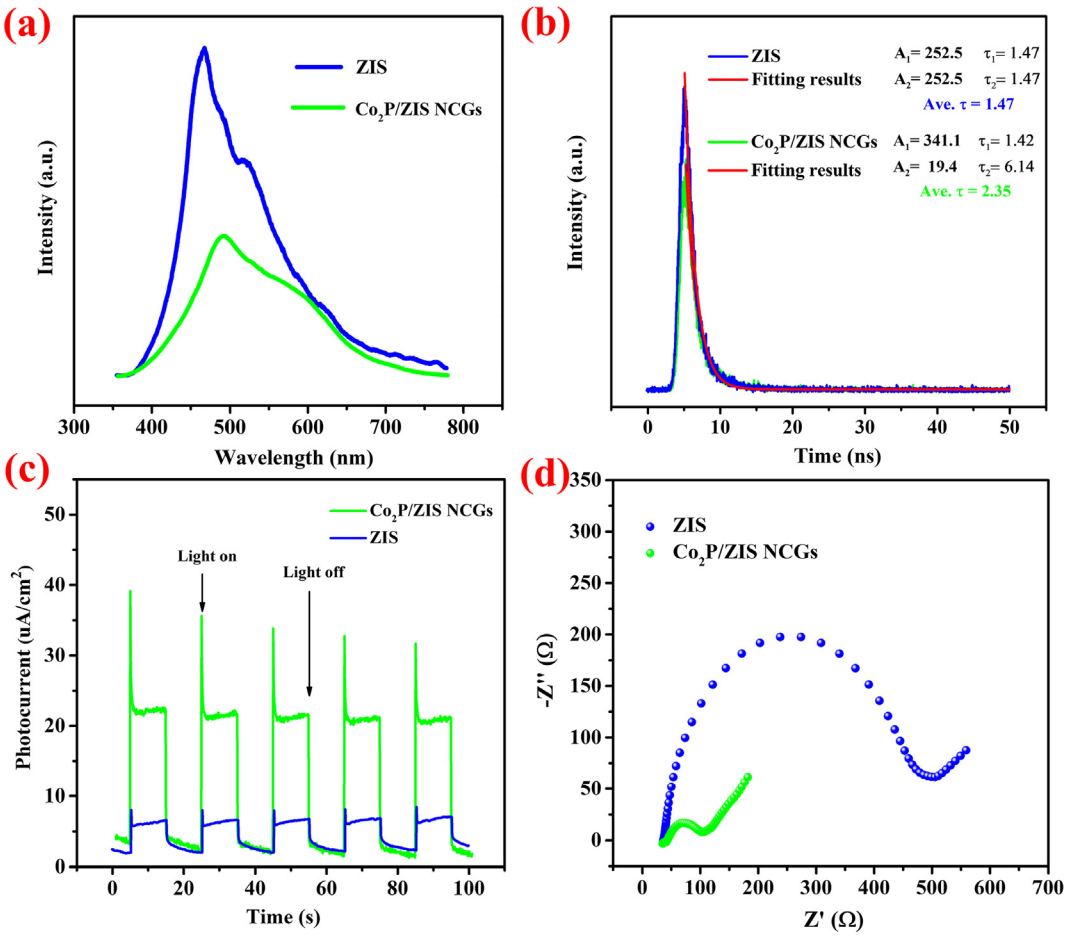

Fig. 6. Steady-state PL spectrum (a), time-resolved PL spectrum (b), transient photocurrent responses (c) and EIS Nyquist plots (d) of pristine ZIS and Co_2P/ZIS NCGs.

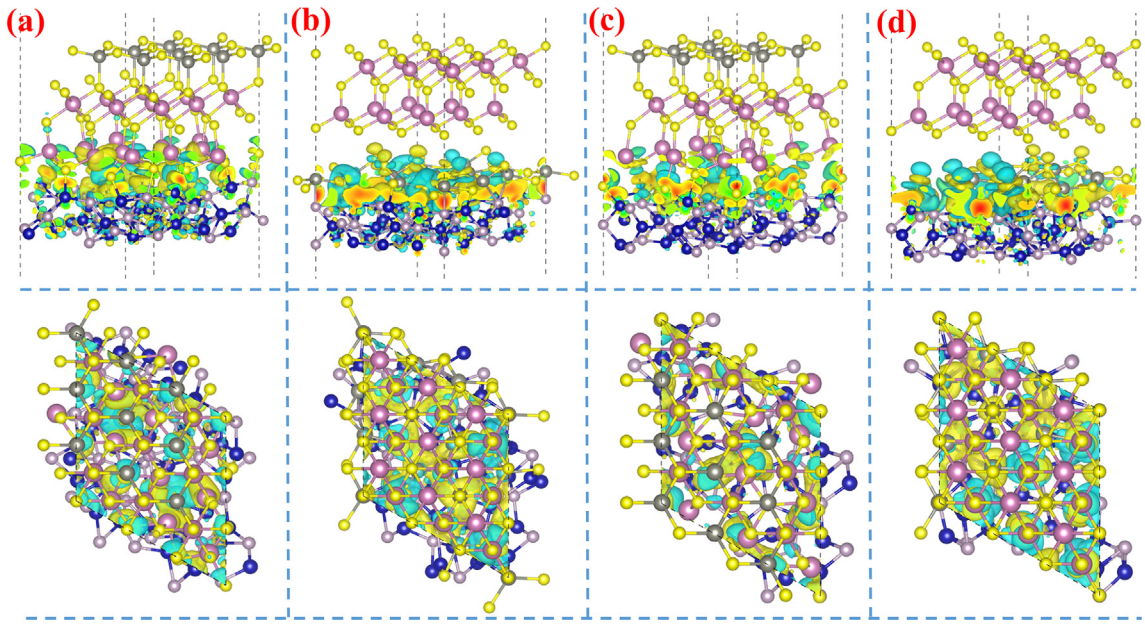

Fig. 7. Four atomically matched interface structures and electron density distributions from front and top views at the interface of $(001)_{Co2P}$ and $(001)_{ZnIn2S4}$ (a-d). The yellow, purple, gray, brown and blue balls was S, In, Zn, P and Co atoms respectively. The yellow and green area represented the accumulated and deficient electron density. (For interpretation of the references to color in this figure legend, the reader is referred to the web version of this article.)

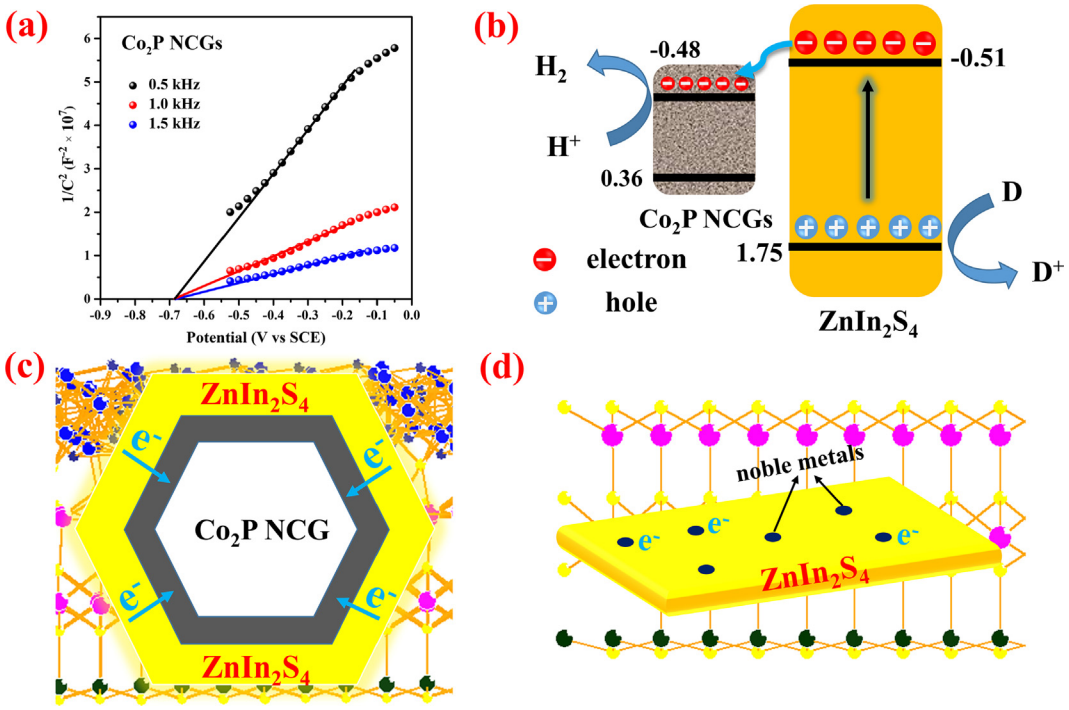

Fig. 8. Mott-Schottky plots of Co_2P (a), electron transfer pathways between Co_2P and ZIS (b), the diffused electron separation over framework of Co_2P/ZIS NCGs (c) and limited active sites over noble metal loaded ZIS samples (d).

4. Conclusions

In summary, a hierarchical $Co_2P/ZnIn_2S_4$ heterojunction was fabricated by coating thin layer of $ZnIn_2S_4$ on the surface of Co_2P nanocages through a facilely hydrothermal method for achieving high efficiently photocatalytic hydrogen evolution (PHE) performance. The unique hollow Co_2P nanocages that derived from ZIF-67 by calcining and phosphiding procedure significantly promoted the separation efficiency of photoinduced electrons and density functional theory (DFT) calculation proved the strong electron transfer from $ZnIn_2S_4$ to Co_2P nanocages at the interfacial heterojunction. PHE results indicated that an efficient rate of 7.93 mmol/g/h over 10% $Co_2P/ZnIn_2S_4$ NCGs with superior stability was achieved, about 10 times higher than that of pristine $ZnIn_2S_4$ and partially relieved the overdependence of noble metals on PHE activity. Therefore, this work demonstrated the feasibility of establishing Co_2P nanocages for boosting charge transfer and introduced a hierarchical $Co_2P/ZnIn_2S_4$ photocatalyst for efficient PHE performance from water without noble metal assisted.

CRediT authorship contribution statement

Quan Zhang: Conceptualization, Methodology, Investigation, Validation, Writing - original draft. **Xiaohao Wang:** Formal analysis, Writing - review & editing. **Juhua Zhang:** Validation. **Lingfeng Li:** Formal analysis. **Huajun Gu:** Investigation, Data curation. **Wei-Lin Dai:** . **:** Funding acquisition, Project administration, Supervision, Writing - review & editing.

Declaration of Competing Interest

The authors declare that they have no known competing financial interests or personal relationships that could have appeared to influence the work reported in this paper.

Acknowledgements

This work was financially supported by Natural Science Foundation of Shanghai (19ZR1403500), National Natural Science Foundation of China (NNSFC, No. 21373054), and Natural Science Foundation of Shanghai Science and Technology Committee (19DZ2270100).

Appendix A. Supplementary material

Supplementary data to this article can be found online at https://doi.org/10.1016/j.jcis.2021.01.083.

References

[1] D. Chen, H. Zhu, S. Yang, N. Li, Q. Xu, H. Li, J. He, J. Lu, Micro-nanocomposites in environmental management, Adv. Mater. 28 (47) (2016) 10443–10458.
[2] Y. Guo, J. Bae, Z. Fang, P. Li, F. Zhao, G. Yu, Hydrogels and hydrogel-derived materials for energy and water sustainability, Chem. Rev. 120 (15) (2020) 7642–7707.
[3] N.S. Lewis, Introduction: Solar energy conversion, Chem. Rev. 115 (2015) 12631–12632.
[4] K. Sayama, Production of high-value-added chemicals on oxide semiconductor photoanodes under visible light for solar chemical-conversion processes, ACS Energy Lett. 3 (5) (2018) 1093–1101.
[5] W. Li, A. Elzatahry, D. Aldhayan, D. Zhao, Core-shell structured titanium dioxide nanomaterials for solar energy utilization, Chem. Soc. Rev. 47 (22) (2018) 8203–8237.
[6] F. Meng, Y. Qin, J. Lu, X. Lin, M. Meng, G. Sun, Y. Yan, Biomimetic design and synthesis of visible-light-driven g-C_3N_4 nanotube @polydopamine/NiCo-layered double hydroxides composite photocatalysts for improved photocatalytic hydrogen evolution activity, J. Colloid Interf. Sci. 584 (2021) 464–473.
[7] X. Qin, H. Li, S. Xie, K. Li, T. Jiang, X.-Y. Ma, K. Jiang, Q. Zhang, O. Terasaki, Z. Wu, W.-B. Cai, Mechanistic analysis-guided Pd-based catalysts for efficient hydrogen production from formic acid dehydrogenation, ACS Catal. 10 (6) (2020) 3921–3932.
[8] L. Sun, Y. Yuan, F. Wang, Y. Zhao, W. Zhan, X. Han, Selective wet-chemical etching to create TiO_2@MOF frame heterostructure for efficient photocatalytic hydrogen evolution, Nano Energy 74 (2020) 104909.
[9] M.Z. Rahman, M.G. Kibria, C.B. Mullins, Metal-free photocatalysts for hydrogen evolution, Chem. Soc. Rev. 49 (6) (2020) 1887–1931.

[10] Y. Li, H. Li, Y. Li, S. Peng, Y.H. Hu, Fe-B alloy coupled with Fe clusters as an efficient cocatalyst for photocatalytic hydrogen evolution, Chem. Eng. J. 344 (2018) 506–513.
[11] D. Xu, P. Xu, Y. Zhu, W. Peng, Y. Li, G. Zhang, F. Zhang, T.E. Mallouk, X. Fan, High yield exfoliation of WS_2 crystals into 1–2 layer semiconducting nanosheets and efficient photocatalytic hydrogen evolution from WS_2/CdS nanorod composites, ACS Appl. Mater. Interfaces 10 (3) (2018) 2810–2818.
[12] Y. Yu, W. Yan, X. Wang, P. Li, W. Gao, H. Zou, S. Wu, K. Ding, Surface engineering for extremely enhanced charge separation and photocatalytic hydrogen evolution on g-C_3N_4, Adv. Mater. 30 (2018) 1705060.
[13] P.-Y. Kuang, P.-X. Zheng, Z.-Q. Liu, J.-L. Lei, H. Wu, N. Li, T.-Y. Ma, Embedding Au quantum dots in rimous cadmium sulfide nanospheres for enhanced photocatalytic hydrogen evolution, Small 12 (48) (2016) 6735–6744.
[14] Y. Pan, M. Wen, Noble metals enhanced catalytic activity of anatase TiO_2 for hydrogen evolution reaction, Int. J. Hydrogen Energy 43 (49) (2018) 22055–22063.
[15] G. Yu, J. Qian, P. Zhang, B. Zhang, G. Liu, Collective excitation of plasmon-coupled Au-nanochain boosts photocatalytic hydrogen evolution of semiconductor, Nat. Commun. 10 (2019) 4912.
[16] Q. Zhang, J. Zhang, L. Zhang, M. Cao, W.L. Dai, Facile construction of flower-like black phosphorus nanosheet@$ZnIn_2S_4$ composite with highly efficient catalytic performance in hydrogen production, Appl. Surf. Sci. 504 (2020) 144366.
[17] Y. Fu, Z. Zhang, C. Zhu, Bicontinuous transition metal phosphides/rGO binder-free electrodes: generalized synthesis and excellent cycling stability for sodium storage, Nanoscale 12 (2020) 16716–16723.
[18] C.C. Weng, J.T. Ren, Z.Y. Yuan, Transition metal phosphide-based materials for efficient electrochemical hydrogen evolution: a critical review, ChemSusChem 13 (2020) 3357–3375.
[19] M.A.R. Anjum, M.S. Okyay, M. Kim, M.H. Lee, N. Park, J.S. Lee, Bifunctional sulfur-doped cobalt phosphide electrocatalyst outperforms allnoble-metal electrocatalysts in alkaline electrolyzer for overall water splitting, Nano Energy 53 (2018) 286–295.
[20] K. Xu, H. Cheng, H. Lv, J. Wang, L. Liu, S. Liu, X. Wu, W. Chu, C. Wu, Y. Xie, Controllable surface reorganization engineering on cobalt phosphide nanowire arrays for efficient alkaline hydrogen evolution reaction, Adv. Mater. 30 (2018) 1703322.
[21] D.A. Reddy, J. Choi, S. Lee, Y. Kim, S. Hong, D.P. Kumar, T.K. Kim, Hierarchical dandelion-flower-like cobalt-phosphide modified CdS/reduced graphene oxide-MoS_2 nanocomposites as a noble-metal-free catalyst for efficient hydrogen evolution from water, Catal. Sci. Technol. 6 (16) (2016) 6197–6206.
[22] P. Wang, T. Wu, Y. Ao, C. Wang, Fabrication of noble-metal-free CdS nanorods-carbon layer-cobalt phosphide multiple heterojunctions for efficient and robust photocatalyst hydrogen evolution under visible light irradiation, Renew. Energy 131 (2019) 180–186.
[23] X. Yue, S. Yi, R. Wang, Z. Zhang, S. Qiu, Cobalt phosphide modified titanium oxide nanophotocatalysts with significantly enhanced photocatalytic hydrogen evolution from water splitting, Small 13 (2017) 1603301.
[24] Z.F. Huang, J. Song, K. Li, M. Tahir, Y.T. Wang, L. Pan, L. Wang, X. Zhang, J.J. Zou, Hollow cobalt-based bimetallic wulfide polyhedra for efficient all-pH-value electrochemical and photocatalytic hydrogen evolution, J. Am. Chem. Soc. 138 (2016) 1359–1365.
[25] Y. Pan, K. Sun, S. Liu, X. Cao, K. Wu, W.C. Cheong, Z. Chen, Y. Wang, Y. Li, Y. Liu, Core-shell ZIF-8@ZIF-67 derived CoP nanoparticles-embedded N-doped carbon nanotube hollow polyhedron for efficient over-all water splitting, J. Am. Chem. Soc. 140 (2018) 2610–2618.
[26] S. Wang, Y. Wang, S.L. Zhang, S. Zang, X.W. Lou, Supporting ultrathin $ZnIn_2S_4$ nanosheets on Co/N-doped graphitic carbon nanocages for efficient photocatalytic H_2 generation, Adv. Mater. 31 (2019) 1903404.
[27] Y. Chen, G. Tian, Z. Ren, K. Pan, Y. Shi, J. Wang, H. Fu, Hierarchical core-shell carbon nanofiber@$ZnIn_2S_4$ composites for enhanced hydrogen evolution performance, ACS Appl. Mater. Interfaces 6 (16) (2014) 13841–13849.
[28] G. Zuo, Y. Wang, W.L. Teo, A. Xie, Y. Guo, Y. Dai, W. Zhou, D. Jana, Q. Xian, W. Dong, Y. Zhao, Ultrathin $ZnIn_2S_4$ nanosheets anchored on $Ti_3C_2T_X$ MXene for photocatalytic H_2 evolution, Angew. Chem. Int. Ed. 59 (28) (2020) 11287–11292.
[29] X. Shi, L. Mao, C. Dai, P. Yang, J. Zhang, F. Dong, L. Zheng, M. Fujitsuka, H. Zheng, Inert basal plane activation of two-dimensional $ZnIn_2S_4$ *via* Ni atom doping for enhanced co-catalyst free photocatalytic hydrogen evolution, J. Mater. Chem. A 8 (26) (2020) 13376–13384.
[30] G. Zhang, D. Chen, N. Li, Q. Xu, H. Li, J. He, J. Lu, Construction of hierarchical hollow Co_9S_8/$ZnIn_2S_4$ tubular heterostructures for highly efficient solar energy conversion and environmental remediation, Angew. Chem. Int. Ed. 59 (21) (2020) 8255–8261.
[31] N. Li, Y. Ding, J. Wu, Z. Zhao, X. Li, Y.-Z. Zheng, M. Huang, X. Tao, Efficient, full spectrum-driven H_2 evolution Z-scheme Co_2P/CdS photocatalysts with Co-S bonds, ACS Appl. Mater. Interfaces 11 (25) (2019) 22297–22306.
[32] S. Li, L. Wang, S. Liu, B. Xu, N. Xiao, Y. Gao, W. Song, L. Ge, J. Liu, In-situ synthesis of strongly coupled Co_2P-CdS nanohybrids: An effective strategy to regulate photocatalytic hydrogen evolution activity, ACS Sustainable Chem. Eng. 6 (2018) 9940–9950.
[33] B. Tian, Z. Li, W. Zhen, G. Lu, Uniformly sized (112) facet Co_2P on graphene for highly effective photocatalytic hydrogen evolution, J. Phys. Chem. C 120 (12) (2016) 6409–6415.
[34] J. Yang, F. Zhang, H. Lu, X. Hong, H. Jiang, Y. Wu, Y. Li, Hollow Zn/Co ZIF particles derived from core-shell ZIF-67@ZIF-8 as selective catalyst for the semi-hydrogenation of acetylene, Angew. Chem. Int. Ed. 54 (37) (2015) 10889–10893.
[35] C. Li, H. Che, P. Huo, Y. Yan, C. Liu, H. Dong, Confinement of ultrasmall $CoFe_2O_4$ nanoparticles in hierarchical $ZnIn_2S_4$ microspheres with enhanced interfacial charge separation for photocatalytic H_2 evolution, J. Colloid Interf. Sci. 581 (2021) 764–773.
[36] Q. Zhang, J. Zhang, L.u. Zhang, F. Yang, L. Li, W.-L. Dai, Black phosphorus quantum dots facilitate carrier separation for enhancing hydrogen production over hierarchical Cu_7S_4/$ZnIn_2S_4$ composites, Catal. Sci. Technol. 10 (4) (2020) 1030–1039.
[37] J. Wang, Y. Chen, W. Zhou, G. Tian, Y. Xiao, H. Fu, H. Fu, Cubic quantum dot/hexagonal microsphere $ZnIn_2S_4$ heterophase junctions for exceptional visible-light-driven photocatalytic H_2 evolution, J. Mater. Chem. A 5 (18) (2017) 8451–8460.
[38] Y. Ye, Z. Zang, T. Zhou, F. Dong, S. Lu, X. Tang, W. Wei, Y. Zhang, Theoretical and experimental investigation of highly photocatalytic performance of CuInZnS nanoporous structure for removing the NO gas, J. Catal. 357 (2018) 100–107.
[39] J. Xu, Y. Qi, L. Wang, In situ derived Ni_2P/Ni encapsulated in carbon/g-C_3N_4 hybrids from metal-organic frameworks/g-C_3N_4 for efficient photocatalytic hydrogen evolution, Appl. Catal. B: Environ. 246 (2019) 72–81.
[40] F. Yang, Q. Zhang, L. Zhang, M. Cao, W. Dai, Facile synthesis of highly efficient Pt/N-rGO/N-$NaNbO_3$ nanorods toward photocatalytic hydrogen production, Appl. Catal. B: Environ. 257 (2019) 117901.
[41] M. Yao, H. Hu, B. Sun, N. Wang, W. Hu, S. Komarneni, Self-supportive mesoporous Ni/Co/Fe phosphosulfide nanorods derived from novel hydrothermal electrodeposition as a highly efficient electrocatalyst for overall water splitting, Small 15 (2019) 1905201.
[42] L. Hu, Y. Hu, R. Liu, Y. Mao, M.-S. Balogun, Y. Tong, Co-based MOF-derived Co/CoN/Co_2P ternary composite embedded in N- and P-doped carbon as bifunctional nanocatalysts for efficient overall water splitting, Int. J. Hydrogen Energy 44 (23) (2019) 11402–11410.
[43] M. Zhu, S. Kim, L. Mao, M. Fujitsuka, J. Zhang, X. Wang, T. Majima, Metal-free photocatalyst for H_2 evolution in visible to near-infrared region: black phosphorus/graphitic carbon nitride, J. Am. Chem. Soc. 139 (2017) 13234–13242.
[44] P. Qiu, C. Xu, N. Zhou, H. Chen, F. Jiang, Metal-free black phosphorus nanosheets-decorated graphitic carbon nitride nanosheets with CP bonds for excellent photocatalytic nitrogen fixation, Appl. Catal. B: Environ. 221 (2018) 27–35.
[45] P. Tan, A. Zhu, L. Qiao, W. Zeng, Y. Ma, H. Dong, J. Xie, J. Pan, Constructing a direct Z-scheme photocatalytic system based on 2D/2D WO_3/$ZnIn_2S_4$ nanocomposite for efficient hydrogen evolution under visible light, Inorg. Chem. Front. 6 (4) (2019) 929–939.
[46] M. Wen, T. Xiong, Z. Zang, W. Wei, X. Tang, F. Dong, Synthesis of MoS_2/g-C_3N_4 nanocomposites with enhanced visible-light photocatalytic activity for the removal of nitric oxide (NO), Opt. Express 24 (2016) 10205–10212.
[47] H. Huang, J. Zhang, L. Jiang, Z. Zang, Preparation of cubic Cu_2O nanoparticles wrapped by reduced graphene oxide for the efficient removal of rhodamine B, J. Alloy. Compd. 718 (2017) 112–115.
[48] T. Hu, K. Dai, J. Zhang, S. Chen, Noble-metal-free Ni_2P modified step-scheme $SnNb_2O_6$/CdS-diethylenetriamine for photocatalytic hydrogen production under broadband light irradiation, Appl. Catal. B: Environ. 269 (2020) 118844.
[49] H. Yu, R. Shi, Y. Zhao, T. Bian, Y. Zhao, C. Zhou, G.I.N. Waterhouse, L.Z. Wu, C.H. Tung, T. Zhang, Alkali-assisted synthesis of nitrogen deficient graphitic carbon nitride with tunable band structures for efficient visible-light-driven hydrogen evolution, Adv. Mater. 29 (2017) 1605148.